

# Calibrationless OSCAR-based Image Reconstruction in Compressed Sensing Parallel MRI

L. El Gueddari <sup>1,2</sup>, P. Ciuciu<sup>1,2</sup>, E. Chouzenoux <sup>3,4</sup>, A. Vignaud <sup>1</sup> and J-C. Pesquet<sup>3</sup>

<sup>1</sup>CEA/NeuroSpin, Gif-sur-Yvette, France

<sup>2</sup>INRIA-CEA Saclay Ile-de-France, Parietal team, Univ Paris-Saclay, France

<sup>3</sup>CVN, Centrale-Supélec, Univ. Paris-Saclay, France

<sup>4</sup>LIGM, Paris-Est University, France

ISBI, 2019, Venice, Italy

# Outline

- 1 Motivation & Context
  - Why non-Cartesian acquisition
  - Non-Cartesian MR mage reconstruction in parallel imaging
- 2 Calibration-less MR image reconstruction
  - Problem statement
  - Joint sparsity regularization
- 3 Experiments & Results
  - Experimental set-up
  - Results
- 4 Conclusion & Discussion

# Outline

- 1 Motivation & Context
  - Why non-Cartesian acquisition
  - Non-Cartesian MR mage reconstruction in parallel imaging
- 2 Calibration-less MR image reconstruction
  - Problem statement
  - Joint sparsity regularization
- 3 Experiments & Results
  - Experimental set-up
  - Results
- 4 Conclusion & Discussion

# Anatomical MRI

Anatomical MRI is generally acquired using Cartesian sampling.

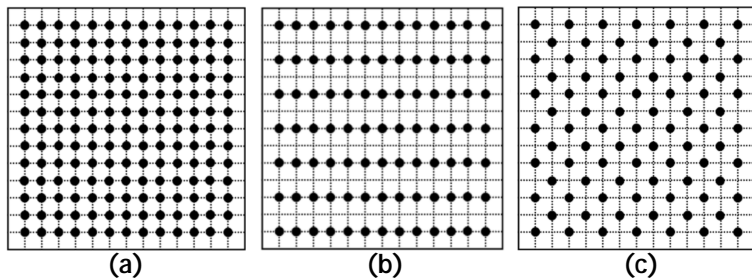


Figure: Typical (a) Cartesian (b) parallel acquisition (c) CAIPIRINHA<sup>1</sup> acquisition

... however in some cases non-Cartesian trajectories are useful ...

<sup>1</sup>Breuer et al. 2006, *Magnetic Resonance in Medicine*.

# Non-Cartesian trajectories for anatomical MRI

A non-exhaustive list of usage

- For ultra-short echo time imaging<sup>2</sup>
- X-nuclei imaging (TPI<sup>3</sup>)
- To correct for motion, especially for abdominopelvic MRI<sup>4</sup>

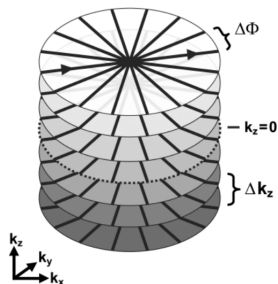


Figure: Stack of stars used for VIBE acquisition

<sup>2</sup>Johnson et al. 2013, *Magnetic Resonance in Medicine*.

<sup>3</sup>Boada et al. 1997, *Magnetic Resonance in Medicine*.

<sup>4</sup>Chandarana et al. 2014, *European radiology*.

# Non-Cartesian trajectories for anatomical MRI

A non-exhaustive list of usage

- For ultra-short echo time imaging<sup>2</sup>
- X-nuclei imaging (TPI<sup>3</sup>)
- To correct for motion, especially for abdominopelvic MRI<sup>4</sup>

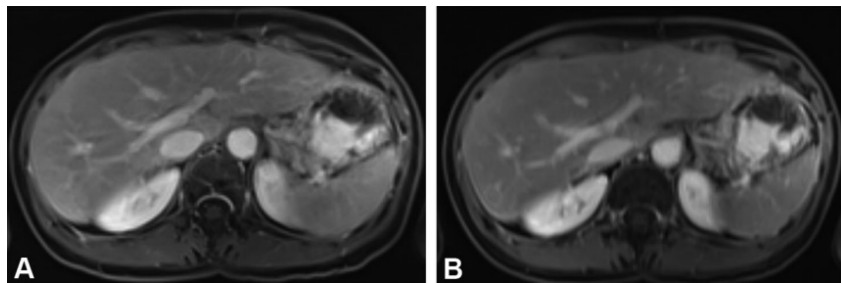


Figure: A: Free-breathing stack-of-stars VIBE, B: Breath-holding conventional VIBE

<sup>2</sup>Johnson et al. 2013, *Magnetic Resonance in Medicine*.

<sup>3</sup>Boada et al. 1997, *Magnetic Resonance in Medicine*.

<sup>4</sup>Chandarana et al. 2014, *European radiology*.

# Non-Cartesian trajectories for anatomical MRI

Renewed interest to speed-up acquisition in the context of Compressed Sensing<sup>5</sup>.

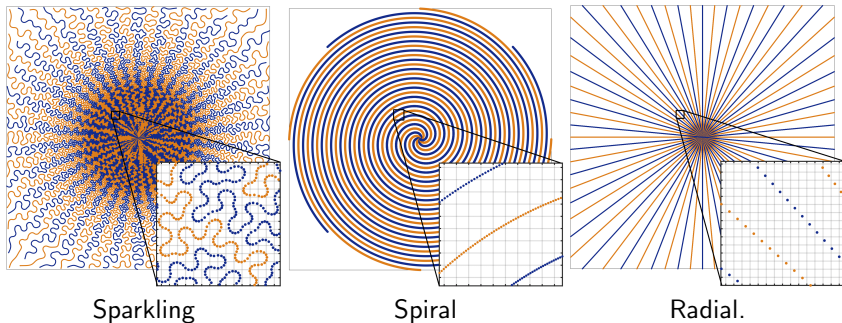


Figure: Example of non-Cartesian trajectories.

<sup>5</sup>Lazarus et al. 2019, *Magnetic Resonance in Medicine*.

# Non-Cartesian trajectories for anatomical MRI

Renewed interest to speed-up acquisition in the context of Compressed Sensing<sup>5</sup>.

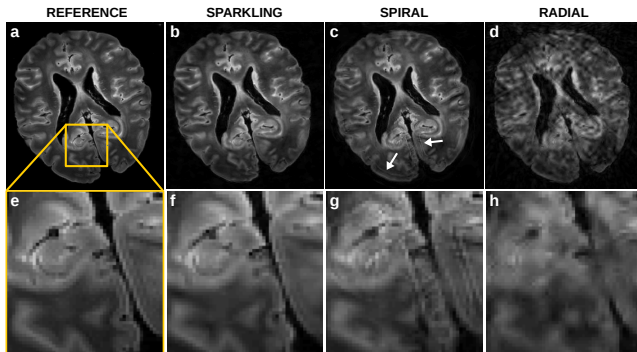


Figure: Comparison of different acquisition trajectories with 16-fold accelerated acquisition on T2\*-weighted images.

<sup>5</sup>Lazarus et al. 2019, *Magnetic Resonance in Medicine*.

# Non-Cartesian trajectories for anatomical MRI

**Parallel imaging acquisition:** collect multiple k-space data using a multi-receiver coil as the latter is known to boost the SNR.



Illustration of multi-receiver coil (phased array).

How do we reconstruct MR images from non-Cartesian k-space measurements in parallel imaging?

# Non-Cartesian MR image reconstruction in parallel imaging

## Self-calibrating methods

Non-Cartesian reconstruction techniques can be split in two categories:

- 1 Self-calibrating methods:

---

<sup>7</sup>Samsonov et al. 2004, *Magnetic Resonance in Medicine*.

<sup>8</sup>Uecker et al. 2014, *Magnetic Resonance in Medicine*.

# Non-Cartesian MR image reconstruction in parallel imaging

## Self-calibrating methods

Non-Cartesian reconstruction techniques can be split in two categories:

① Self-calibrating methods:

- require a region where the signal has been sampled at least at the Nyquist rate

---

<sup>7</sup>Samsonov et al. 2004, *Magnetic Resonance in Medicine*.

<sup>8</sup>Uecker et al. 2014, *Magnetic Resonance in Medicine*.

# Non-Cartesian MR image reconstruction in parallel imaging

## Self-calibrating methods

Non-Cartesian reconstruction techniques can be split in two categories:

### 1 Self-calibrating methods:

- require a region where the signal has been sampled at least at the Nyquist rate
- model the coil sensitivity profiles  $S_\ell$  for all channels  $\ell = 1, \dots, L$ <sup>7,8</sup>

---

<sup>7</sup>Samsonov et al. 2004, *Magnetic Resonance in Medicine*.

<sup>8</sup>Uecker et al. 2014, *Magnetic Resonance in Medicine*.

# Non-Cartesian MR image reconstruction in parallel imaging

## Self-calibrating methods

Non-Cartesian reconstruction techniques can be split in two categories:

### 1 Self-calibrating methods:

- require a region where the signal has been sampled at least at the Nyquist rate
- model the coil sensitivity profiles  $S_\ell$  for all channels  $\ell = 1, \dots, L$ <sup>7,8</sup>
- solve an inverse problem and recover a single full FOV image:

$$\hat{\mathbf{x}} = \arg \min_{\mathbf{x} \in \mathbb{C}^N} \frac{1}{2} \sum_{\ell=1}^L \sigma_\ell^2 \|\mathbf{F}_\Omega \mathbf{S}_\ell \mathbf{x} - \mathbf{y}_\ell\|_2^2 + \lambda \|\mathbf{x}\|_1 \quad (1)$$

<sup>7</sup>Samsonov et al. 2004, *Magnetic Resonance in Medicine*.

<sup>8</sup>Uecker et al. 2014, *Magnetic Resonance in Medicine*.

# Non-Cartesian MR image reconstruction in parallel imaging

## Self-calibrating methods

Non-Cartesian reconstruction techniques can be split in two categories:

### 1 Self-calibrating methods:

- require a region where the signal has been sampled at least at the Nyquist rate
- model the coil sensitivity profiles  $S_\ell$  for all channels  $\ell = 1, \dots, L$ <sup>7,8</sup>
- solve an inverse problem and recover a single full FOV image:

$$\hat{\mathbf{x}} = \arg \min_{\mathbf{x} \in \mathbb{C}^N} \frac{1}{2} \sum_{\ell=1}^L \sigma_\ell^2 \|\mathbf{F}_\Omega \mathbf{S}_\ell \mathbf{x} - \mathbf{y}_\ell\|_2^2 + \lambda \|\mathbf{x}\|_1 \quad (1)$$

Note: Extraction of coil sensitivity maps is challenging in non-Cartesian case

<sup>7</sup>Samsonov et al. 2004, *Magnetic Resonance in Medicine*.

<sup>8</sup>Uecker et al. 2014, *Magnetic Resonance in Medicine*.

# Non-Cartesian MR Image reconstruction from multi-channel array coil acquisition

## Calibration-less methods

Non-Cartesian reconstruction techniques can be split in two categories:

- 2 Calibration-less methods:
  - do not require any calibration region

---

<sup>9</sup>Trzasko and Manduca 2011, *Signals, Systems and Computers (ASILOMAR)*, 2011 Conference Record of the Forty Fifth Asilomar Conference on.

<sup>10</sup>Majumdar and Ward 2012, *Magnetic Resonance in Medicine*.

# Non-Cartesian MR Image reconstruction from multi-channel array coil acquisition

## Calibration-less methods

Non-Cartesian reconstruction techniques can be split in two categories:

### 2 Calibration-less methods:

- do not require any calibration region
- solve an inverse problem but recover channel-specific images

---

<sup>9</sup>Trzasko and Manduca 2011, *Signals, Systems and Computers (ASILOMAR)*, 2011 Conference Record of the Forty Fifth Asilomar Conference on.

<sup>10</sup>Majumdar and Ward 2012, *Magnetic Resonance in Medicine*.

# Non-Cartesian MR Image reconstruction from multi-channel array coil acquisition

## Calibration-less methods

Non-Cartesian reconstruction techniques can be split in two categories:

### 2 Calibration-less methods:

- do not require any calibration region
- solve an inverse problem but recover channel-specific images
- use the redundant information given by each coil to impose constraints such as low-rank CLEAR<sup>9</sup> or group-sparsity CALM<sup>10</sup>

---

<sup>9</sup>Trzasko and Manduca 2011, *Signals, Systems and Computers (ASILOMAR), 2011 Conference Record of the Forty Fifth Asilomar Conference on*.

<sup>10</sup>Majumdar and Ward 2012, *Magnetic Resonance in Medicine*.

# Non-Cartesian MR Image reconstruction from multi-channel array coil acquisition

## Calibration-less methods

Non-Cartesian reconstruction techniques can be split in two categories:

### 2 Calibration-less methods:

- do not require any calibration region
- solve an inverse problem but recover channel-specific images
- use the redundant information given by each coil to impose constraints such as low-rank CLEAR<sup>9</sup> or group-sparsity CALM<sup>10</sup>
- more likely to be used for on-line image reconstruction

---

<sup>9</sup>Trzasko and Manduca 2011, *Signals, Systems and Computers (ASILOMAR)*, 2011 Conference Record of the Forty Fifth Asilomar Conference on.

<sup>10</sup>Majumdar and Ward 2012, *Magnetic Resonance in Medicine*.

# Outline

- 1 Motivation & Context
  - Why non-Cartesian acquisition
  - Non-Cartesian MR mage reconstruction in parallel imaging
- 2 Calibration-less MR image reconstruction
  - Problem statement
  - Joint sparsity regularization
- 3 Experiments & Results
  - Experimental set-up
  - Results
- 4 Conclusion & Discussion

# Problem statement

Calibration-less MR image reconstruction problem solved using an *analysis formulation*:

## Definition

MR image reconstruction is formulated as follows:

$$\hat{\underline{x}} = \arg \min_{\underline{x} \in \mathbb{C}^{N \times L}} \left\{ \frac{1}{2} \sum_{\ell=1}^L \sigma_{\ell}^2 \|F_{\Omega} \mathbf{x}_{\ell} - \mathbf{y}_{\ell}\|_2^2 + g(\mathbf{T} \underline{x}) \right\}, \quad (2)$$

with:

- $\mathbf{y}_{\ell} \in \mathbb{C}^M$  the  $\ell^{\text{th}}$  channel-specific data set
- $\mathbf{x}_{\ell} \in \mathbb{C}^N$  the  $\ell^{\text{th}}$  channel-specific reconstructed image (ex.  $N = 512 \times 512$ )
- $F_{\Omega}$  is the forward under-sampling Fourier operator
- $\mathbf{T} \in \mathbb{C}^{N_{\psi} \times N}$  linear operator related to a sparse decomposition
- $g$  is a convex regularization term that promotes sparsity

# Optimization algorithm

## Primal dual optimization

We aim to find:

$$\hat{\underline{x}} \underset{\underline{x} \in \mathcal{C}^{N \times L}}{\text{argmin}} [f(\underline{x}) + g(\mathbf{T}\underline{x})] \quad (3)$$

where:

- $f$  is convex, differentiable on  $\mathcal{C}^{N \times L}$  and its gradient is  $\beta$ -Lipschitz
- $g \in \Gamma_0(\mathcal{C}^{N_\Psi \times L})$  with a closed form proximity operator, given by:

$$\text{prox}_g(\underline{z}) = \underset{\underline{v} \in \mathcal{C}^{N_\Psi \times L}}{\text{argmin}} \frac{1}{2} \|\underline{z} - \underline{v}\|^2 + g(\underline{v}) \quad (4)$$

Note: Those are standard assumption in optimization based image reconstruction methods.

# Optimization algorithm

## Condat-Vũ sequence

Using a primal-dual optimization method proposed by Condat-Vũ<sup>11,12</sup>:

### Algorithm 1: Condat-Vũ algorithm

```
initialize  $k = 0, \tau > 0, \kappa > 0, \underline{x}_0, \underline{z}_0$ ;  
while  $k < K$  do  
     $\underline{x}_{k+1} := \underline{x}_k - \tau (\nabla f(\underline{x}_k) + \mathbf{T} \underline{z}_k)$ ;  
     $\underline{w}_{k+1} := \underline{z}_k + \kappa \mathbf{T} (2\underline{x}_{k+1} - \underline{x}_k)$ ;  
     $\underline{z}_{k+1} := \underline{w}_{k+1} - \kappa \operatorname{prox}_{g/\kappa} \left( \frac{\underline{w}_{k+1}}{\kappa} \right)$ ;  
end
```

with:

- the algorithm weakly converges to the solution of Eq. (3) if

$$\frac{1}{\tau} - \kappa \|\mathbf{T}\|^2 \geq \frac{\beta}{2}$$

- $\tau$  and  $\kappa$  hyper-parameters set as follows:  $\tau := \frac{1}{\beta}$ ,  $\kappa := \frac{\beta}{2\|\mathbf{T}\|^2}$

<sup>11</sup>Condat 2013, *Journal of Optimization Theory and Applications*.

<sup>12</sup>Vũ 2013, *Advances in Computational Mathematics*.

# Joint sparsity regularization

## Group-LASSO

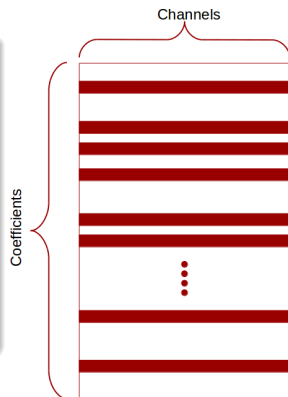
Parallel imaging has been proved to have tighter recovery guarantees than single channel acquisition when combined with Group-LASSO (GL) regularization<sup>13</sup>.

### Definition

The group-LASSO penalty is defined as follows:

$$g_{GL}(\underline{z}) = k\underline{z}k_{1,2} = \sum_{s=1}^S \left( \lambda \gamma^s \sum_{p=1}^{P_s} \sqrt{\sum_{\ell=1}^L |z_{s\ell p}|^2} \right)$$

- $\lambda$  and  $\gamma$  are positive hyper-parameters
- $s$  models the scale or subband dependence



<sup>13</sup>Chun, Adcock, and Talavage 2016, *IEEE Transactions on Medical Imaging*.

For  $\gamma = 1$  the algorithm corresponds to Majumdar and Ward, *Magnetic Resonance in Medicine*, 2012

# Joint sparsity regularization

## Sparse group-LASSO

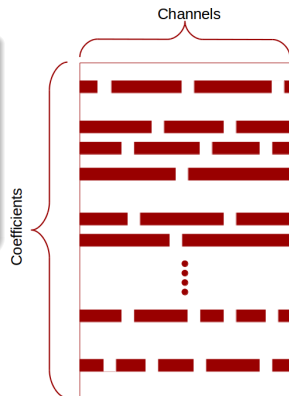
Variant: Sparse group-LASSO<sup>15</sup> (sGL)

### Definition

$$\forall \underline{z} \in \mathbb{R}^{N_\Psi}, g_{\text{sGL}}(\underline{z}) = g_{\text{GL}}(\underline{z}) + \mu \|\underline{z}\|_{k_1} \quad (5)$$

- $\mu$  being positive hyper-parameter.

sGL proximity operator<sup>18</sup> is closed form and corresponds to the composition of GL proximity operator with soft-thresholding.



<sup>15</sup>Friedman, Hastie, and Tibshirani 2010, *arXiv preprint arXiv:1001.0736*.

# Joint sparsity regularization

## Octagonal Shrinkage and Clustering Algorithm for Regression

Inferring the structure via a pairwise  $\ell_1$  norm.  
OSCAR regularization<sup>16</sup>:

### Definition

$$\begin{aligned} g_{\text{OSCAR}}(\mathbf{z}) &= \sum_{s=1}^S \lambda \left[ \sum_{j=1}^{P_s L} j z_{sj} + \gamma \sum_{j < k} \max\{j z_{sj}, j z_{sk}\} \right] \\ &= \sum_{s=1}^S \lambda \left[ \sum_{j=1}^{P_s L} (\gamma(j-1) + 1) j z_{sj} \right] \end{aligned} \quad (6)$$

where:

- $\mathbf{z}_{\#} \in \mathbb{R}^{N \times L}$  the wavelet coefficients sorted in decreasing order, i.e.:  
 $\mathbf{z}_{\#} = [z_{s1}, \dots, z_{sP_s L}]$ .
- $\lambda$  and  $\gamma$  are some positive hyper-parameters that need to be set

<sup>16</sup>Bondell and Reich 2008, *Biometrics*.

# Outline

- 1 Motivation & Context
  - Why non-Cartesian acquisition
  - Non-Cartesian MR mage reconstruction in parallel imaging
- 2 Calibration-less MR image reconstruction
  - Problem statement
  - Joint sparsity regularization
- 3 Experiments & Results
  - Experimental set-up
  - Results
- 4 Conclusion & Discussion

# Experimental set-up

Sequence parameters:

- Ex-vivo baboon brain
- 7T Siemens Scanner GRE
- 1Tx/32Rx Nova coil
- Sparkling trajectory
- $390\mu\text{m}$   $390\mu\text{m}$  in plane-resolution
- 3mm slice thickness
- Acceleration factor of 15 in time
- Under-sampling factor of 2.5
- $T$ : Undecimated Bi-Orthogonal 7-9 wavelet transform

Hyper-parameters set using a grid-search procedure.

Cartesian scan  $512 \times 512$  was acquired and used for reference.

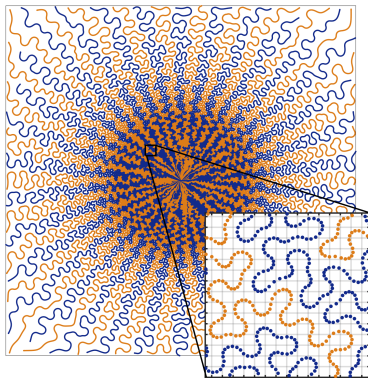


Figure: Sparkling trajectory

# Results

## Quantitative assessment

Coil combination: Square root of the Sum-Of-Squares  
Structural SIMilarity Index (SSIM)<sup>17</sup> used to set hyper-parameters

Table: Image quality assessment for all regularizers.

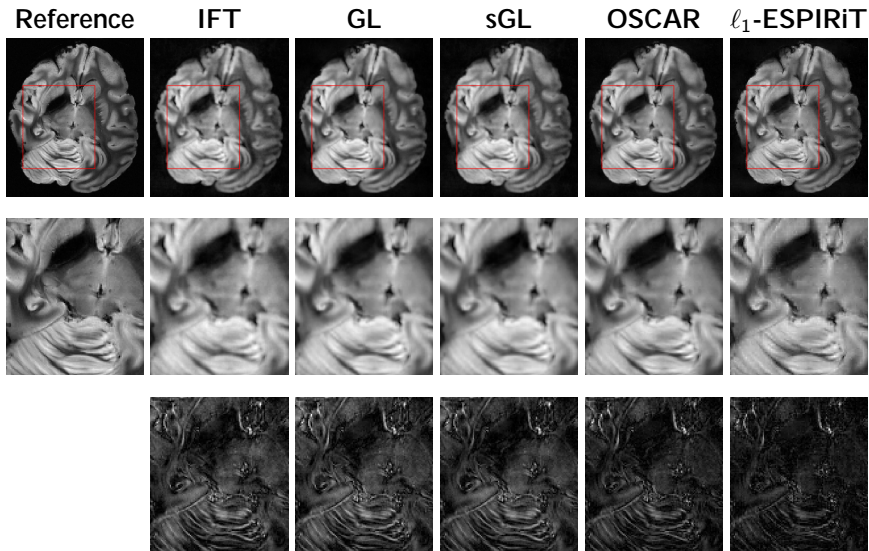
	SSIM	pSNR (dB)	NRMSE
IFT	0.847	26.50	0.263
GL	0.864	26.92	0.254
sGL	0.851	26.77	0.259
OSCAR	<b>0.875</b>	<b>30.49</b>	<b>0.177</b>
$\ell_1$ -ESPIRiT	0.874	28.32	0.238

Note:  $\ell_1$ -ESPIRiT is a self-calibrating method.

<sup>17</sup>Wang et al. 2004, *IEEE transactions on image processing*.

# Results

## Comparison of the Sum-Of-Squares



# Results

## Quantitative assessment

Comparison between coil images:

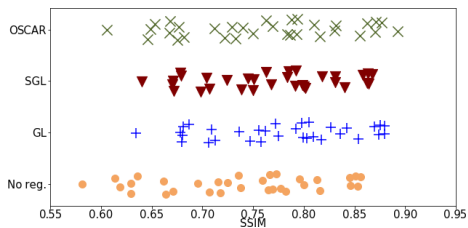


Figure: Assessment of the SSIM score per channel.

# Results

## Quantitative assessment

Comparison between coil images:

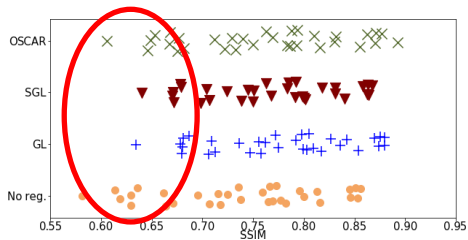
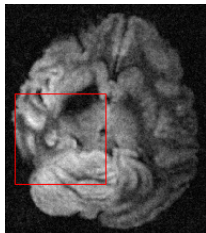


Figure: Assessment of the SSIM score per channel.

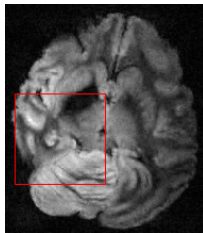
# Results

Comparison of the image channels: low-SNR channel

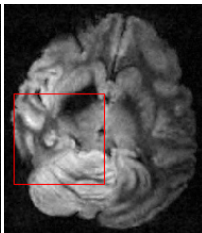
No reg.  
SSIM= 0.630



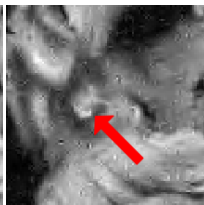
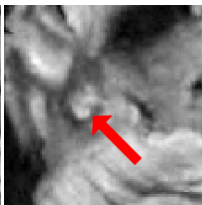
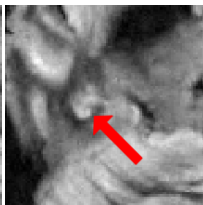
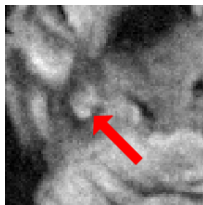
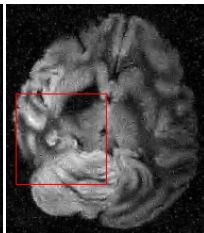
Group-LASSO  
SSIM= 0.680



Sparse GL  
SSIM= 0.672



OSCAR  
SSIM= 0.646



# Results

## Quantitative assessment

Comparison between coil images:

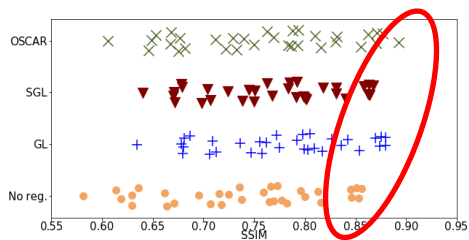


Figure: Assessment of the SSIM score per channel.

# Results

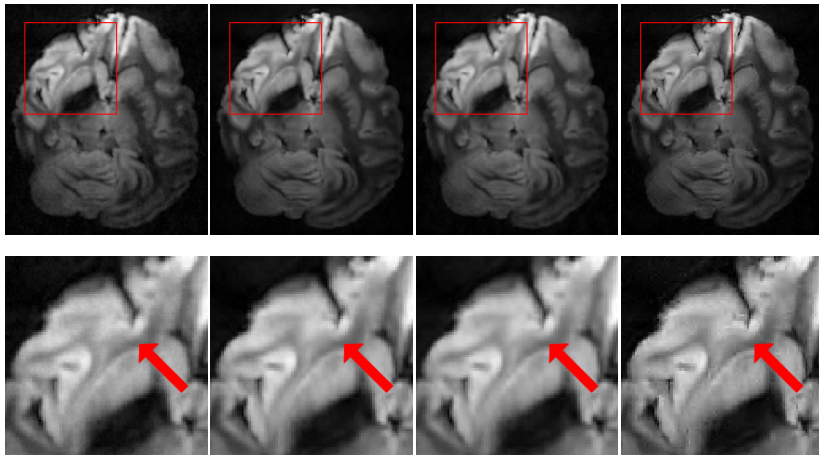
Comparison of the image channels: high-SNR channel

No reg.  
SSIM= 0.846

Group-LASSO  
SSIM= 0.880

Sparse GL  
SSIM= 0.863

OSCAR  
SSIM= 0.893



# Outline

- 1 Motivation & Context
  - Why non-Cartesian acquisition
  - Non-Cartesian MR mage reconstruction in parallel imaging
- 2 Calibration-less MR image reconstruction
  - Problem statement
  - Joint sparsity regularization
- 3 Experiments & Results
  - Experimental set-up
  - Results
- 4 Conclusion & Discussion

# Conclusion & Discussion

## Conclusion:

- New parallel CS-MRI reconstruction algorithm
- No sensitivity maps
- OSCAR outperforms group-LASSO and sparse group-LASSO
- OSCAR and  $\ell_1$ -ESPIRiT are comparable, however the latest is self-calibrating
- Same optimization method to solve calibration-less MR reconstruction

## Perspective:

- Extension to 3D-MRI
- Study motion impact on the reconstruction

- Boada, Fernando E. et al. (1997). “Fast three dimensional sodium imaging”. In: *Magnetic Resonance in Medicine* 37.5, pp. 706–715.
- Bondell, H.D. and B.J. Reich (2008). “Simultaneous regression shrinkage, variable selection, and supervised clustering of predictors with OSCAR”. In: *Biometrics* 64.1, pp. 115–123.
- Breuer, Felix A et al. (2006). “Controlled aliasing in volumetric parallel imaging (2D CAIPIRINHA)”. In: *Magnetic Resonance in Medicine* 55.3, pp. 549–556.
- Chandarana, Hersh et al. (2014). “Free-breathing contrast-enhanced T1-weighted gradient-echo imaging with radial k-space sampling for paediatric abdominopelvic MRI”. In: *European radiology* 24.2, pp. 320–326.
- Chun, I.Y., B. Adcock, and T.M. Talavage (2016). “Efficient compressed sensing SENSE pMRI reconstruction with joint sparsity promotion”. In: *IEEE Transactions on Medical Imaging* 35.1, pp. 354–368.
- Condat, L. (2013). “A primal–dual splitting method for convex optimization involving Lipschitzian, proximable and linear composite terms”. In: *Journal of Optimization Theory and Applications* 158.2, pp. 460–479.
- Friedman, J., T. Hastie, and R. Tibshirani (2010). “A note on the group lasso and a sparse group lasso”. In: *arXiv preprint arXiv:1001.0736*.

- Johnson, Kevin M. et al. (2013). “Optimized 3D ultrashort echo time pulmonary MRI”. In: *Magnetic Resonance in Medicine* 70.5, pp. 1241–1250.
- Lazarus, Carole et al. (2019). “SPARKLING: variable-density k-space filling curves for accelerated T2\*-weighted MRI”. In: *Magnetic Resonance in Medicine* 81.6, pp. 3643–3661.
- Majumdar, A.I and R.K. Ward (2012). “Calibration-less multi-coil MR image reconstruction”. In: *Magnetic Resonance in Medicine* 30.7, pp. 1032–1045.
- Roemer, P.B. et al. (1990). “The NMR phased array”. In: *Magnetic Resonance in Medicine* 16.2, pp. 192–225.
- Samsonov, Alexei A et al. (2004). “POCSSENSE: POCS-based reconstruction for sensitivity encoded magnetic resonance imaging”. In: *Magnetic Resonance in Medicine* 52.6, pp. 1397–1406.
- Trzasko, J.D. and A. Manduca (2011). “Calibrationless parallel MRI using CLEAR”. In: *IEEE*, pp. 75–79.
- Uecker, M. et al. (2014). “ESPIRiT– an eigenvalue approach to autocalibrating parallel MRI: where SENSE meets GRAPPA”. In: *Magnetic Resonance in Medicine* 71.3, pp. 990–1001.
- Vũ, BC (2013). “A splitting algorithm for dual monotone inclusions involving cocoercive operators”. In: *Advances in Computational Mathematics* 38.3, pp. 667–681.

Wang, Zhou et al. (2004). “Image quality assessment: from error visibility to structural similarity”. In: *IEEE transactions on image processing* 13.4, pp. 600–612.